arXiv:1704.06295v1 [nucl-th] 20 Apr 2017

Standardized Cumulants of Flow Harmonic Fluctuations

Navid Abbasi[1],* Davood Allahbakhshi[1],† Ali Davody[1,2],‡ and Seyed Farid Taghavi[1]§
[1] *School of Particles and Accelerators, Institute for Research in Fundamental Sciences (IPM), P.O. Box 19395-5531, Tehran, Iran and*
[2] *Institute of Theoretical Physics, Regensburg University, 93040 Regensburg, Germany*

The distribution of flow harmonics in heavy ion experiment can be characterized by standardized cumulants. We first use the Elliptic-Power distribution together with the hydrodynamic linear response to study the two dimensional standardized cumulants of elliptic and triangular flow (v_2 and v_3) distribution. Using this, the $2q$-particle correlation functions $c_3\{2\}$, $c_3\{4\}$ and $c_3\{6\}$, are related to the second, forth and sixth standardized cumulants of the v_3 distribution, respectively. The $c_n\{2q\}$ can be also written in terms of cumulants $v_n\{2q\}$. Specifically, $-(v_3\{4\}/v_3\{2\})^4$ turns out to be the kurtosis of the v_3 event-by-event fluctuation distribution. We introduce a new probability distribution $p(v_3)$ with $v_3\{2\}$, kurtosis and sixth order standardized cumulant as its free parameters. Compared to the Gaussian distribution, it indicates a more accurate fit with experimental results. Finally, we compare the kurtosis obtained from simulation with that of extracted from experimental data for the v_3 distribution.

I. INTRODUCTION

There is a strong belief that the matter produced in the heavy ion collision experiments in both Relativistic Heavy Ion Collider (RHIC) and the Large Hadron Collider (LHC) has a collective behavior. This is experimentally confirmed by measuring the second Fourier harmonic of the particle momentum azimuthal distribution, namely the *elliptic flow*, v_2 [1, 2]. In fact, the almond shape of the initial energy density in non-central collisions manifests itself in v_2. Moreover, there exist other *flow harmonics* (Fourier harmonics) such as triangle flow, v_3 [3] which corresponds to the event-by-event position fluctuations of nucleons inside the nucleus. The triangular flow as well as other flow harmonics have been observed in RHIC [4, 5] and LHC [6–9].

The reaction plane angle in a single collision is not an accurate observable in the experiments. If we had prior knowledge about the reaction plane, we would obtain different values for each flow harmonic of the events in the same centrality class. However, one would still be able to extract the flow harmonics of many events in the same centrality class with even unknown reaction plane angle. One way to do that is to use the multiparticle azimuthal correlation function, $c_n\{2k\}$ [10, 11].

In [12], it is shown that the fluctuations of initial anisotropy ε_n, generated by different initial condition Monte-Carlo generators, can be described by Elliptic-Power distribution. This distribution is not exact Gaussian. As a result, after the hydrodynamic evolution, we also expect that the v_n distribution of an ensemble of events in the same centrality class not to be exactly Gaussian. Certain statistical quantities such as skewness, kurtosis, etc. quantify the deviation of a given distribution from Gaussianity. It has been shown that the fine splitting between $v_2\{4\}$ and $v_2\{6\}$ is the consequence of the skewness in v_2 distribution [13].

In this work, to study the distribution of v_2 we first use a simple model of heavy ion collision, the Elliptic-Power distribution together with the linear response of hydrodynamics. It turns out that by considering $c_2\{2\}$ to $c_2\{8\}$, the only quantity which can be experimentally extracted from v_2 distribution would be the skewness. We also show that for v_3 distribution, both ratios $-(v_3\{4\}/v_3\{2\})^4$ and $4(v_3\{6\}/v_3\{2\})^6$ are indicating the deviation of v_3 distribution from Gaussianity. Similar quantities have been studied before in [14, 15], however, here, we find their relation with standardized cumulants as well. In addition, we introduce a new distribution function $p(v_3)$ (see (35)) which has a small deviation from Gaussianity, identified by two standardized cumulants. These cumulants can be found by fitting the v_3 distribution with experimental data. Finally, in a more realistic model, we use iEBE-VISHNU event generator [16] and compare the kurtosis of v_3, found by event generator with that of obtained from experimental data.

II. ELLIPTIC-POWER DISTRIBUTION

In this section, we will review a simple and interesting model of the heavy-ion collision initial state, introduced in [12, 17, 18]. Consider N independent point-like sources distributed in a two dimensional plane with a 2D-Gaussian probability distribution. This distribution function could have different widths along two directions. We can imagine the sources as the location of nucleon-nucleon collision in the Glauber model. Using this distribution, as we will see in the following, one can find a distribution for the initial anisotropy ε_n which is called the Elliptic-Power distribution. Although this model is more simple than MC-Glauber [19–21], MC-KLN [22, 23] and IP-Glasma [24] models, it has been shown in [12] that the Elliptic-Power distribution fits perfectly with the ε_n

* Abbasi@ipm.ir
† Allahbakhshi@ipm.ir
‡ Davody@ipm.ir
§ s.f.taghavi@ipm.ir

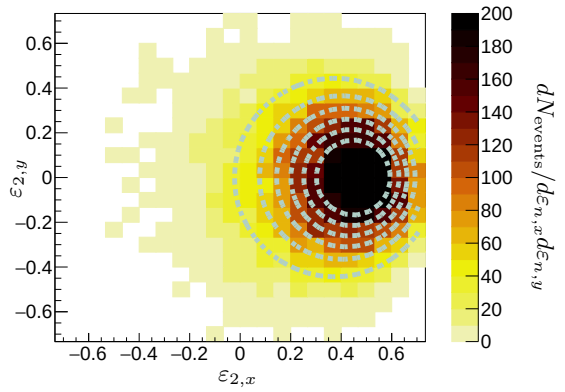

(a)

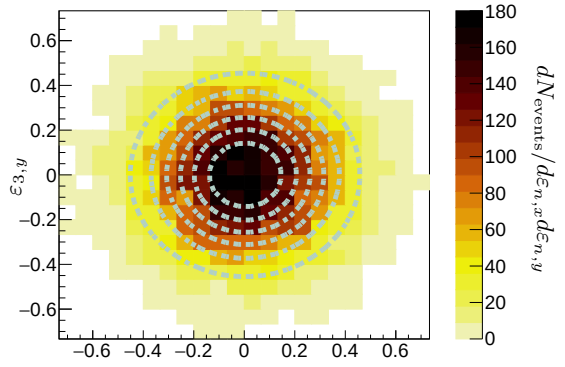

(b)

FIG. 1. (Color online) The eccentricity and triangularity distribution of 14000 events for MC-Glauber model in 50 - 55% centrality class of Pb-Pb collision, generated by iEBE-VISHNU (yellow spectrum). The Elliptic-Power distribution (4) is indicated by Light-Blue dashed contours. The ellipticity and power are obtained by fitting: (a) $n = 2$, $\alpha = 8.70$ and $\varepsilon_0 = 0.40$ (b) $n = 3$, $\alpha = 9.54$ and $\varepsilon_0 = 0.00$.

distribution generated by the more complex models.

In this model, the energy density is given by

$$\rho(X,Y) = \rho_0 \sum_{i=1}^{N} \delta(X - X_i)\delta(Y - Y_i) \qquad (1)$$

where (X_i, Y_i) is the position of i^{th} source on the plane. In order to quantify the shape of each randomly generated event, we use the 2D Fourier analysis of $\rho(X,Y)$ developed in [25]. Introducing the averaging over energy density of a single event

$$\{\cdots\} = \frac{\int \cdots \rho(X,Y)dXdY}{\int \rho(X,Y)dXdY},$$

we define the complex quantity $\boldsymbol{\varepsilon}_n$ as

$$\boldsymbol{\varepsilon}_n = \varepsilon_n e^{in\Phi_n} \equiv \frac{\{r^n e^{in\varphi}\}}{\{r^n\}}, \qquad (2)$$

where r and φ are radial and azimuthal coordinates in X-Y plane. For $n = 1$ in this relation, we have to replace r by r^3 [25][1]. Occasionally, we use the Cartesian notation wherein $\varepsilon_{n,x} = \varepsilon_n \cos n\Phi_n$ and $\varepsilon_{n,y} = \varepsilon_n \sin n\Phi_n$. Using (1), we can specifically find $\varepsilon_{2,x}$ and $\varepsilon_{2,y}$ as follows,

$$\varepsilon_{2,x} = \frac{\sum_{i=1}^{N}(X_i^2 - Y_i^2)}{\sum_{i=1}^{N}(X_i^2 + Y_i^2)}, \quad \varepsilon_{2,y} = \frac{2\sum_{i=1}^{N} X_i Y_i}{\sum_{i=1}^{N}(X_i^2 + Y_i^2)}. \qquad (3)$$

The above $\varepsilon_{2,x}$ is indicating that how much the randomly generated event is almond shape while, $\varepsilon_{2,y}$ shows that how much the almond is rotated in the X-Y plane. In [17, 18], it has bee shown that if we randomly generate several events with specific width of Gaussian distribution, then the probability distribution of events with respect to $\varepsilon_{2,x}$ and $\varepsilon_{2,y}$ is given by

$$p(\varepsilon_{n,x}, \varepsilon_{n,y}) = \frac{\alpha}{\pi}(1 - \varepsilon_0^2)^{\alpha+1/2} \frac{(1 - \varepsilon_{n,x}^2 - \varepsilon_{n,y}^2)^{\alpha-1}}{(1 - \varepsilon_0 \varepsilon_{n,x})^{2\alpha+1}}. \qquad (4)$$

In the above, we follow [12] and use ε_n not only for $n = 2$, but also for $n > 2$. This relation is called *Elliptic-Power* distribution. In this distribution, the *ellipticity* ε_0 and *power* $\alpha = (N-1)/2$ are two unknown free parameters. Note that for $\alpha \gg 1$, this distribution reduces to a 2D Gaussian distribution.

In [12], the parameters ε_0 and α are obtained by fitting the function (4) with the azimuthally integrated distributions generated by different models. As we expect, the result depends on the model we are studying and also on the value of n. It is worth to mention that for ε_3 the best fit is obtained by setting $\varepsilon_0 = 0$, because, we do not expect any average value for this parameter. Specifically, if we set $\varepsilon_0 = 0$ and integrate over φ then we find the *Power* distribution [27]

$$p(\varepsilon_n) = 2\alpha\varepsilon_n(1 - \varepsilon_n^2)^{\alpha-1}. \qquad (5)$$

Here we calculate the ε_0 and α without integrating over the azimuthal angle in (4). We generate up to 14000 initial states of Pb-Pb collision with center of mass energy $\sqrt{s} = 2.76$ TeV using MC-Glauber model implemented in iEBE-VISHNU generator [16]. To find the ε_0 and α, we fit (4) with the distribution found by filling a 2D histogram of $\varepsilon_{n,x}$ and $\varepsilon_{n,y}$. In Fig.1, we have depicted the histogram and Elliptic-Power distribution for 50 - 55% centrality class. The result for harmonic $n = 2$ is $\alpha = 8.70$, $\varepsilon_0 = 0.40$, while for $n = 3$ is $\alpha = 9.54$, $\varepsilon_0 = 0.00$. We show that by increasing the centrality, α decreases, in agreement with [12] (see Fig.2(a)).

For $n = 2$, it is already well-known [12, 13] that the distribution is left-skewed in the $\varepsilon_{2,x}$ direction. We

[1] The other method to characterize the initial conditions is using the Bessel-Fourier modes [26]. The advantage of using these modes is that they are making a complete basis and the fluid dynamic evolution can be studied for each mode separately.

have demonstrated this result in a two dimensional histogram in Fig.1(a). For $n = 3$ however, ε_0 is almost zero (Fig.2(b)) and in this case, no apparent skewness[2] is observed in the distribution. Although it is not exactly clear why the MC-Glauber distribution is skewed, we can still explain it for the Elliptic-Power distribution as follows: suppose the sources are distributed via a 2D Gaussian with the width in the x axis (σ_x) being larger than that in the y axis (σ_y) and also with the vanishing cross term. The latter means the larger axis of the almond is fixed along the x axis. Using these assumptions, it turns out that the average of $\varepsilon_{2,y}$ is equal to zero while $\varepsilon_{2,x}$ gets a non-zero average.

Based on the above assumptions, no skewness would be observed in the y direction while the distribution is skewed in the x direction. The reason for the latter statement is as follows. The distribution along the y axis is narrower than that of along the x axis. In other words, the sources are more probable to be generated along the x axis rather than the y axis. Therefore, the distribution of the $\varepsilon_{2,x}$ is more concentrated on the right side of the average which means that it is left-skewed. For central collisions (or for $n = 3$ in Fig.1(b)) with $\langle\varepsilon_{2,x}\rangle = 0$ the distribution in Fig.1(a) becomes rotationally symmetric and consequently non-skewed.

III. CUMULANT ANALYSIS OF PROBABILITY DISTRIBUTION

In the previous section, we observed that the Elliptic-Power distribution is skewed for $\varepsilon_0 \neq 0$ and the same feature was observed for the MC-Glauber. In order to study the distribution of ε_n (and flow harmonics) we employ the cumulant analysis. We first review the terminology used in the present work and then find the explicit form of standardized cumulants (will be defined shortly) of the Elliptic-Power distribution.

A. Cumulants: Review and Terminology

The cumulants of a distribution $\mathcal{P}(\xi)$ are obtained from the generating function $\log\langle e^{\lambda\xi}\rangle$. If we expand this function around $\lambda = 0$ then the cumulant κ_n will be the coefficient of the $\lambda^n/n!$. The advantages of using cumulants instead of moments are that they are homogeneous, shift invariant (except κ_1) and $\kappa_{n\geq 3} = 0$ for the normal distribution.

In statistics, the standardized central moments $\gamma_1 = \langle(\xi - \langle\xi\rangle)^3\rangle/\sigma^3$ and $K = \langle(\xi - \langle\xi\rangle)^4\rangle/\sigma^4$ are called skewness and kurtosis respectively. Recalling $\kappa_2 \equiv \sigma^2$, one can simply see that $\gamma_1 = \kappa_3/\kappa_2^{3/2}$ and $K = \kappa_4/\kappa_2^2 + 3$.

[2] We define the skewness systematically in section III.

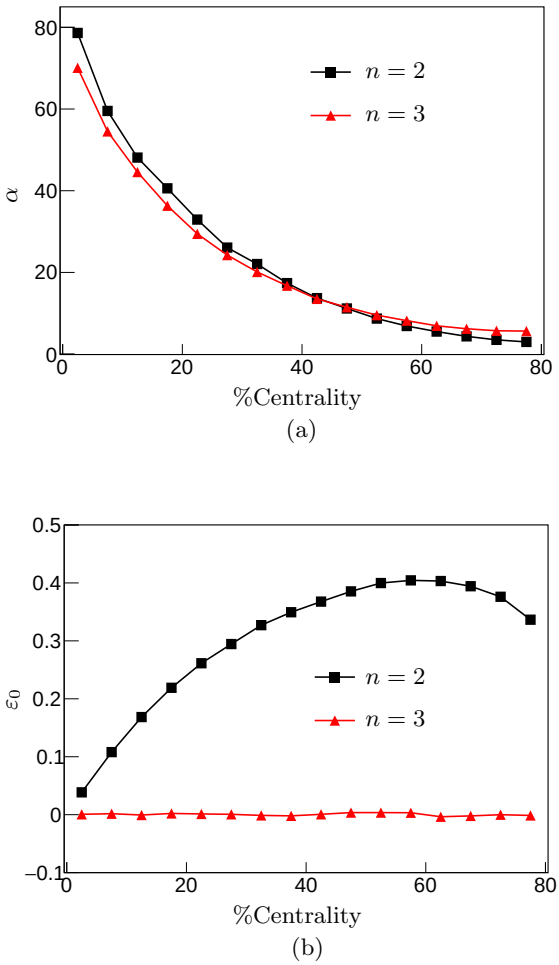

FIG. 2. (Color online) The power (a) and ellipticity (b) obtained by fitting (4) with MC-Glauber initial states for harmonics $n = 2, 3$.

According to the properties of the cumulants, the kurtosis of a Gaussian distribution is equal to 3. For this reason, it is common to call $\gamma_2 = K - 3$ as the kurtosis. We will use the latter terminology in this work. In general, we define the standardized cumulants of a distribution as follows,

$$\gamma_{q-2} = \frac{\kappa_q}{\kappa_2^{q/2}}. \tag{6}$$

In most part of this paper, we deal with two dimensional distributions and therefore need to use the 2D (standardized) cumulants. Similar to the 1D case, we can find the cumulants by expanding the following generating function,

$$\log\langle e^{\lambda_x\xi_x+\lambda_y\xi_y}\rangle = \sum_{m,n=0} \frac{\lambda_x^m\lambda_y^n}{m!n!}\mathcal{A}_{mn}, \tag{7}$$

where (ξ_x, ξ_y) is a 2D random variable with a 2D distri-

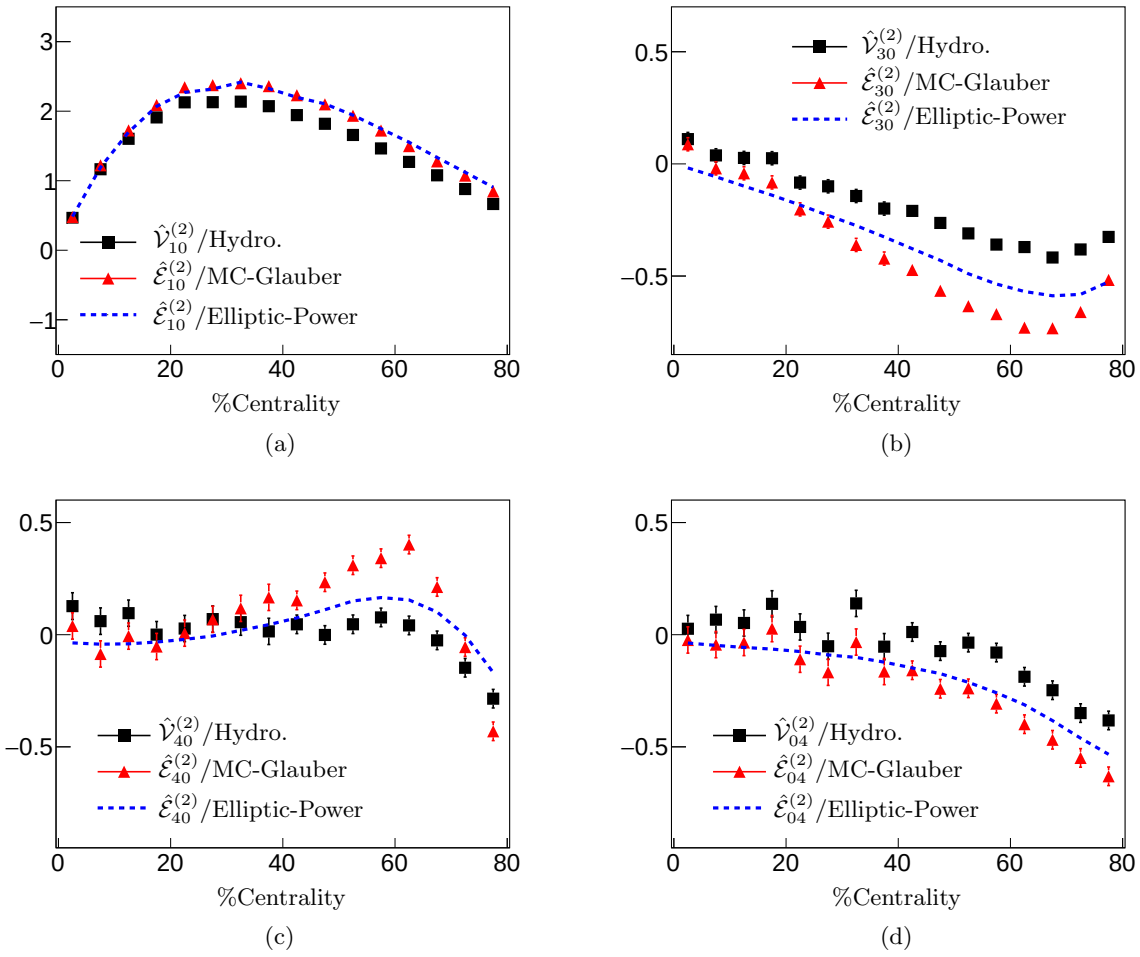

FIG. 3. (Color online) Some non-zero standardized cumulants obtained from event-by-event fluctuation distribution. The blue dashed curve and red dots are related to the initial anisotropy ε_2 distribution acquired from Elliptic-Power distribution and MC-Glauber respectively. The black dots are standardized cumulates of v_2 distribution. The error bars indicate the statistical errors.

bution function $\mathcal{P}(\xi_x, \xi_y)$[3]. From (7), $\mathcal{A}_{mn}$ is found in terms of the moments $\langle \xi_x^p \xi_y^q \rangle$ [4]. In the following, we call $m+n$ as the order of the $\mathcal{A}_{mn}$ cumulant. It is worth to mention that the cumulants of a normal distribution with order higher than two are equal to zero. Also it can be shown that the cumulant statistical error of a sample with N entries, is proportional to $\frac{1}{N}$ [5].

In order to generalize the notion of skewness, kurtosis, etc., into 2D dimensions, we can simply replace (6) with the following expression

$$\hat{\mathcal{A}}_{mn} = \frac{\mathcal{A}_{mn}}{\sqrt{\mathcal{A}_{20}^m \mathcal{A}_{02}^n}}, \tag{8}$$

where clearly we have $\hat{\mathcal{A}}_{20} = \hat{\mathcal{A}}_{02} = 1$. In the following, we call $\hat{\mathcal{A}}_{mn}$ as (2D) standardized cumulants.

B. Moments and Cumulants of Elliptic-Power Distribution

Now we specifically concentrate on the cumulants of the Elliptic-Power distribution. We show the cumulant obtained from ε_n distribution by $\mathcal{E}_{kl}^{(n)}$. In order to find $\mathcal{E}_{kl}^{(n)}$, we first have to compute the moments of distribu-

[3] In this manuscript, we refer to $\mathcal{A}_{mn}$ as the *cumulant* and to the $c_n\{2k\}$ as $2k$-particle correlation function.
[4] In Ref.[13], $\mathcal{A}_{30}$ and $\mathcal{A}_{12}$ are shown by s_1 and s_2 respectively.
[5] The method of finding the explicit form of the errors can be found in the statistic textbooks such as Ref.[28]

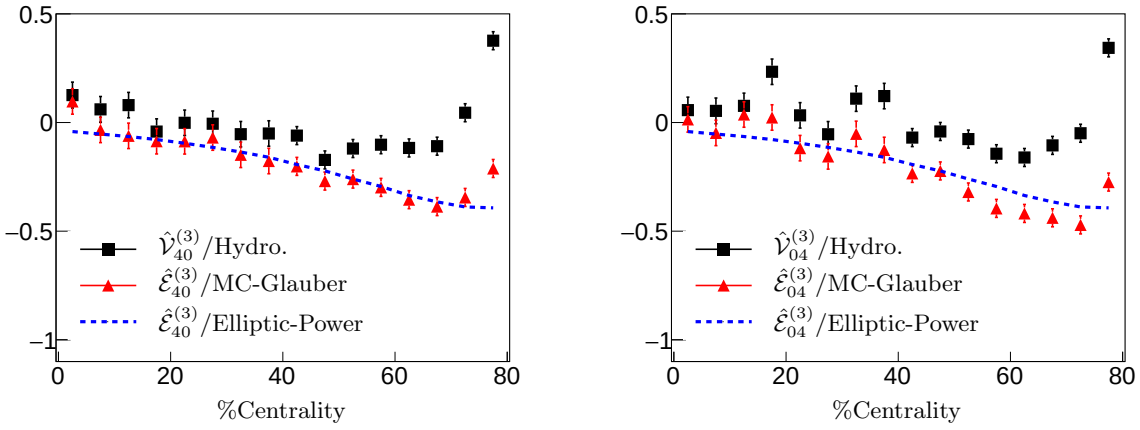

FIG. 4. (Color online) Similar to Fig.3 for $n = 3$.

tion:

$$\langle \varepsilon_{n,x}^k \varepsilon_{n,y}^l \rangle = \int d\varepsilon_{n,x} d\varepsilon_{n,y}\, \varepsilon_{n,x}^k \varepsilon_{n,y}^l\, p(\varepsilon_{n,x}, \varepsilon_{n,y}). \quad (9)$$

By considering the symmetries of (4), some of the moments identically vanish. Let us recall that for $n = 2$ the ε_0 is non-zero for non-central collisions, hence, the probability $p(\varepsilon_{2,x}, \varepsilon_{2,y})$ is not symmetric under $\varepsilon_{2,x} \to -\varepsilon_{2,x}$ in this case. However, $p(\varepsilon_{2,x}, \varepsilon_{2,y})$ is an even function with respect to parameter $\varepsilon_{2,y}$ which immediately leads to $\langle \varepsilon_{2,x}^k \varepsilon_{2,y}^{2l+1} \rangle = 0$. Under the above considerations, if we use the explicit form of the cumulants by extracting them from (7), we find $\mathcal{E}_{21}^{(2)} = \mathcal{E}_{03}^{(2)} = 0$.

On the other hand, for $n = 3$ we have $\varepsilon_0 \simeq 0$ which means $p(\varepsilon_{3,x}, \varepsilon_{3,y})$ is even with respect to both parameters $\varepsilon_{3,x}$ and $\varepsilon_{3,y}$. Consequently, the only non-zero moments are $\langle \varepsilon_{2,x}^{2k} \varepsilon_{2,y}^{2l} \rangle$. In other words, for $n = 3$, all odd order cumulants are equal to zero, i.e. $\mathcal{E}_{kl}^{(3)} = 0$ for $k + l = 2q + 1$. As a result, the non-zero and non-trivial standardized cumulants appear from the forth order. For $\boldsymbol{\varepsilon}_3$, the other observation from (4) is that it is symmetric with respect to $\varepsilon_{3,x} \leftrightarrow \varepsilon_{3,y}$ which means $\mathcal{E}_{kl}^{(3)} = \mathcal{E}_{lk}^{(3)}$.

In general, we can find the moments of the Elliptic-Power distribution analytically. Introducing the following integral

$$I_m(q, \alpha, \beta) = \int_{-1}^{1} dx\, \frac{x^m (1 - x^2)^\alpha}{(1 - qx)^\beta}, \quad (10)$$

we are able to write the moments (9) as follows

$$\langle \varepsilon_{n,x}^k \varepsilon_{n,y}^l \rangle = \frac{\alpha}{\pi} (1 - \varepsilon_0^2)^{\alpha + 1/2} \times I_m(\varepsilon_0, \alpha + \frac{n-1}{2}, 2\alpha + 1)\; I_n(0, \alpha - 1, 0). \quad (11)$$

The integral $I_m(q, \alpha, \beta)$ has analytical solution in terms of the hypergeometric functions (see Appendix A). Using this together with (7), one can find cumulants of the Elliptic-Power distribution straightforwardly.

Let us now study the implications of the above discussion to the case of heavy ion collisions. We know that in this case, both ε_0 and α depend on the centrality (Fig.2). Having known the centrality dependence of ε_0 and α, we would obtain semi-analytical cumulants which can be used as a model for describing the heavy ion collision initial state.

C. Cumulants: Elliptic-Power Vs MC-Glauber

Now we compare the cumulants $\hat{\mathcal{E}}_{kl}^{(n)}$ calculated analytically form Elliptic-Power distribution with those of extracted from MC-Glauber. The results are depicted in Fig.3 for $n = 2$ and Fig.4 for $n = 3$. In these figures, the red triangles are obtained from MC-Glauber distribution and the error bars indicate the statistical errors. Here, the centrality parameter between 0 to 80% is divided into 16 bins. For each bin in the range of 0-40% and 40-80%, 7000 and 14000 events are generated by iEBE-VISHNU respectively (see section V for more details). In the same figures mentioned above, the blue dashed curve demonstrates the cumulants extracted from the Elliptic-Power distribution. To find them, we have used the equations (A4)-(A6) with α and ε_0 obtaining from MC-Glauber initial states fit.

Note that when finding the cumulants of Elliptic-Power distribution, we have found a large number of outputs, a set of cumulants, from a lower number of inputs of the MC-Glauber, namely α and ε_0.

The standardized cumulant $\hat{\mathcal{E}}_{30}^{(2)}$ is exactly the skewness parameter defined in Ref.[12] and the plot in the panel (b) of Fig.3 is coincident with Fig.2 in [12]. In agreement with the symmetries of the Elliptic-Power distribution, we have $\hat{\mathcal{E}}_{01}^{(2)} \simeq \hat{\mathcal{E}}_{11}^{(2)} \simeq \hat{\mathcal{E}}_{01}^{(2)} \simeq \hat{\mathcal{E}}_{21}^{(2)} \simeq \hat{\mathcal{E}}_{03}^{(2)} \simeq \hat{\mathcal{E}}_{31}^{(2)} \simeq \hat{\mathcal{E}}_{13}^{(2)} \simeq 0$. Moreover, we checked that for MC-

Glauber model $\hat{\mathcal{E}}^{(2)}_{12} \sim \hat{\mathcal{E}}^{(2)}_{22} \sim 0$. In short, up to forth order, we consider the following standardized cumulants for $n = 2$,

$$\begin{aligned} &\hat{\mathcal{E}}^{(2)}_{10} \gtrsim \mathcal{O}(1), \\ &\hat{\mathcal{E}}^{(2)}_{30}, \quad \hat{\mathcal{E}}^{(2)}_{40}, \quad \hat{\mathcal{E}}^{(2)}_{04} \sim \mathcal{O}(10^{-1}). \end{aligned} \tag{12}$$

However, we will see later that the magnitude of the standardized cumulants are increasing with the order of cumulants. In section IV, we will discuss the order of magnitude of the standardized cumulants in detail.

For $n = 3$ in Fig.4, all the cumulants extracted from Elliptic-Power distribution up to order three are equal to zero. This feature also is observed for the cumulants extracted from MC-Glauber. We have checked that, it is a reasonable assumption to consider $\hat{\mathcal{E}}^{(3)}_{22} \sim 0$. Also the cumulants $\hat{\mathcal{E}}^{(3)}_{40}$ and $\hat{\mathcal{E}}^{(3)}_{04}$ are almost equal. Note that it is an exact equality for the cumulants extracted from Elliptic-Power distribution. In other words, except $\hat{\mathcal{E}}^{(3)}_{20}$ and $\hat{\mathcal{E}}^{(3)}_{02}$, there is only one independent normalized cumulant in $n = 3$ harmonics, $\hat{\mathcal{E}}^{(3)}_{40} \sim \hat{\mathcal{E}}^{(3)}_{04}$, in agreement with the Elliptic-Power distribution.

D. Cumulants of Collision Final State

The momentum distribution of the particles observed in the detector is correlated with the heavy ion collision initial state. Here, we will try to clarify the relation between the cumulants obtained from initial distribution and the final state particle distribution.

The azimuthal distribution of particles is analyzed via Fourier analysis

$$\frac{2\pi}{N}\frac{dN}{d\phi} = 1 + \sum_{n=1}^{\infty} 2v_n \cos\left[n(\phi - \psi_n)\right]. \tag{13}$$

Defining the complex flow harmonics $\boldsymbol{v}_n = v_n e^{in\psi_n}$, we can find $\boldsymbol{v}_n = \langle e^{in\phi}\rangle_s$ where $\langle\cdots\rangle_s$ is averaging in a single event. Instead of using the complex form of the flow harmonics, we occasionally use the Cartesian form of them defined as follows

$$v_{n,x} = v_n \cos(n\psi_n), \quad v_{n,x} = v_n \sin(n\psi_n). \tag{14}$$

Each non-vanishing $\boldsymbol{v}_n$ measures how non-uniform, the final particle distribution is. For example, the ellipticity of the initial state produced in the non-central collisions is manifested in the non-zero values for $v_{2,x}$ and $v_{2,y}$.

Note that the azimuthal angle of the reaction plane ψ_2 is not a direct observable in the experiment. However, in simulation the reaction plane angle is under the control such that we may fix it as $\psi_2 = 0$. Doing so and also neglecting the fluctuations, $v_{2,y}$ turns out to be zero. If we take the fluctuations into account, however, this will be no longer zero. For the same reason, the flow harmonics $v_{n,x}$ and $v_{n,y}$ for $n \neq 2$ are also non-vanishing.

So far, we have discussed the flow harmonics in a single event. In an ensemble of many events in the same centrality class, the flow harmonics produce a distribution $p(v_{n,x}, v_{n,y})$. As a result, one can find the cumulants of this distribution via (7) similar to what we have done for ε_n distribution. We will refer to the cumulants extracted from $p(v_{n,x}, v_{n,y})$ as $\mathcal{V}^{(n)}_{kl}$.

In the experiment, although the angle ψ_n is not known, we are still able to find the parameter v_n in each centrality class by studying the $2q$-particle correlation functions $c_n\{2q\}$ [10]. In [11], the relation between $2q$-particle correlation functions and v_n is found,

$$\sum_q \frac{\lambda^{2q}}{(q!)^2} c_n\{2q\} = \log I_0(\lambda v_n). \tag{15}$$

In the following, we refer to v_n obtained by equating the coefficients of λ^{2q} in two sides, as $v_n\{2q\}$[6].

In order to relate the $c_n\{2q\}$ with the cumulant $\mathcal{V}^{(n)}_{kl}$, one has to compare the ψ_n integrated of (7) with (15) [11, 13]. We can set $\lambda_x = \lambda\cos\psi_n$ and $\lambda_y = \lambda\sin\psi_n$ in (7) and define the generating function $G(\lambda)$ as

$$\log G(\lambda) = \log\left(\int_0^{2\pi} \frac{d\psi_n}{2\pi} \langle e^{\lambda(v_{n,x}\cos\psi_n + v_{n,y}\sin\psi_n)}\rangle\right). \tag{17}$$

Consequently, one can find the relation between $c_n\{2q\}$ (or $v_n\{2q\}$) with $\mathcal{V}^{(n)}_{pq}$ by equating the expansions of $\log I_0(\lambda v_n)$ and $\log G(\lambda)$.

After some calculations, one simply finds that the general form of the $c_n\{2k\}$ in terms of $\mathcal{V}_{pq}$ has the following structure[7] [8],

$$c_n\{2k\} = \sum_{\{\alpha_i, p_i, q_i\}} a_{\{\alpha_i,p_i,q_i\}} \mathcal{V}^{\ell_1}_{p_1 q_1} \cdots \mathcal{V}^{\ell_N}_{p_N q_N}, \tag{18}$$

where

$$\sum_{i=1}^{N} \ell_i(p_i + q_i) = 2k. \tag{19}$$

---

[6] From (15), one finds explicitly

$$v_n^2\{2\} \equiv c_n\{2\}, \quad v_n^4\{4\} \equiv -c_n\{4\}, \quad v_n^6\{6\} \equiv c_n\{6\}/4 \tag{16}$$

[7] We occasionally ignore the superscript (n) in the 2D cumulants for simplicity in notation.

[8] In the following, we present two explicit examples:

$$\begin{aligned} c_n\{2\} &= \mathcal{V}^2_{01} + \mathcal{V}^2_{10} + \mathcal{V}_{02} + \mathcal{V}_{20}, \\ c_n\{4\} &= -\mathcal{V}^4_{01} - 2\mathcal{V}^2_{10}\mathcal{V}^2_{01} + 2\mathcal{V}_{02}\mathcal{V}^2_{01} - 2\mathcal{V}_{20}\mathcal{V}^2_{01} + 4\mathcal{V}_{03}\mathcal{V}_{01} \\ &\quad + 8\mathcal{V}_{10}\mathcal{V}_{11}\mathcal{V}_{01} + 4\mathcal{V}_{21}\mathcal{V}_{01} - \mathcal{V}^4_{10} + \mathcal{V}^2_{02} - 2\mathcal{V}_{02}\mathcal{V}^2_{10} + 4\mathcal{V}^2_{11} \\ &\quad + \mathcal{V}^2_{20} + \mathcal{V}_{04} + 4\mathcal{V}_{10}\mathcal{V}_{12} + 2\mathcal{V}^2_{10}\mathcal{V}_{20} - 2\mathcal{V}_{02}\mathcal{V}_{20} + 2\mathcal{V}_{22} \\ &\quad + 4\mathcal{V}_{10}\mathcal{V}_{30} + \mathcal{V}_{40}. \end{aligned}$$

The constraint (19) is found by the following argument. Clearly, $\mathcal{V}_{mn}$ given by (7) is homogeneous. Consider the rescaling $\xi_i \to \alpha\xi_i$ for $i = x, y$. Then one can assume that ξ_i is unchanged and $\lambda_i \to \alpha\lambda_i$ in the left hand side of the equation (7). Now in order to find same cumulant by equating two sides of the equation, we need to have $\mathcal{A}_{mn} \to \alpha^{m+n}\mathcal{A}_{mn}$. Recall that $c_n\{2k\}$ can be obtained by integrating the azimuthal angle of the left hand side of (7). As a result, we expect the similar scaling for them, $c_n\{2k\} \to \alpha^{2k}c_n\{2k\}$. By using these ingredients, one can find the constraint (19).

Because of the averaging over ψ_n, there are more informations about event-by-event fluctuations in $\mathcal{V}_{pq}^{(n)}$ rather than $c_n\{2k\}$. In the following sections of this work, we would like to find the informations encoded in $\mathcal{V}_{pq}^{(n)}$ from $c_n\{2k\}$ as much as possible. If one obtains $c_n\{2k\}$ explicitly in terms of $\mathcal{V}_{pq}^{(n)}$ then it can be seen that the number of terms in $c_n\{2k\}$ grows rapidly with increasing q. In the following section, we will argue how to truncate $c_n\{2k\}$ expansion.

IV. ELLIPTIC-POWER DISTRIBUTION AND CUMULANT EXPANSION TRUNCATION

In the previous section, we showed that, in principle, one would be able to obtain $c_n\{2k\}$ in terms of cumulants $\mathcal{V}_{pq}^{(n)}$. The former is an experimental observable while the latter can be obtained from simulation. On the other hand, one knows that the Elliptic-Power distribution can explain the distribution of $\boldsymbol{\varepsilon}_n$ obtained from more sophisticated initial condition models. This distribution leads to a semi-analytical result for $\hat{\mathcal{E}}_{pq}^{(n)}$. The semi-analytical $\hat{\mathcal{E}}_{pq}^{(n)}$ can be considered as $\hat{\mathcal{V}}_{pq}^{(n)}$, by using the hydrodynamic linear response approximation. Consequently we may use the Elliptic-Power distribution as a toy model to find a good approximation for truncating the expansion (18).

The hydrodynamic response to the initial state has been studied from different directions [25, 29–33]. However, it is a reasonable approximation for $n = 2, 3$ to consider the hydrodynamic response being linear [25, 29, 31, 33],

$$\boldsymbol{v}_n \simeq \alpha_n \boldsymbol{\varepsilon}_n, \tag{20}$$

where α_n is a real valued constant of proportionality. With this approximation and using the homogeneity of cumulants, we immediately find

$$\mathcal{V}_{pq}^{(n)} \simeq \alpha_n^{p+q}\mathcal{E}_{pq}^{(n)}. \tag{21}$$

Referring to the definition of standardized cumulants (8), we see that at the linear approximation

$$\hat{\mathcal{V}}_{pq}^{(n)} \simeq \hat{\mathcal{E}}_{pq}^{(n)}. \tag{22}$$

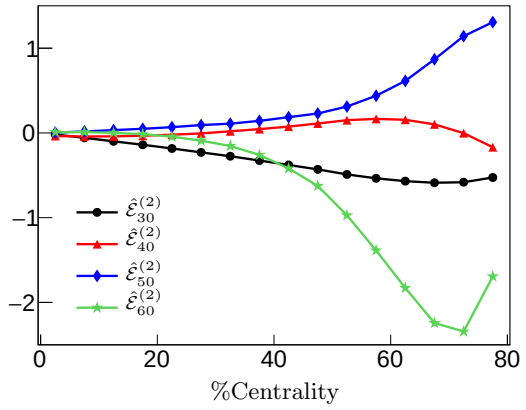

(a)

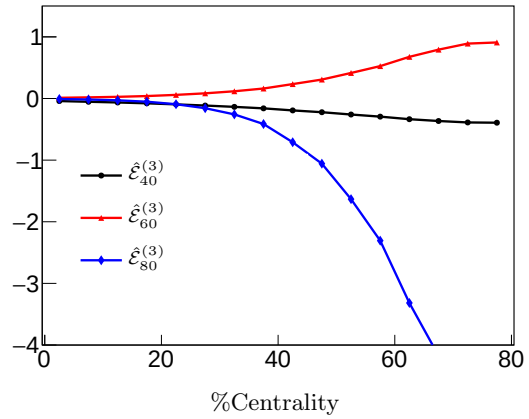

(b)

FIG. 5. (Color online) A few leading standardized cumulants obtained from Elliptic-Power distribution for (a) $n = 2$ and (b) $n = 3$. Typically by increasing the order, the value of the cumulants increase.

A. Standardized Cumulant Order of Magnitude

Let us remind that in (18), the $2q$-particle correlation function, $c_n\{2q\}$, was given in terms of $\mathcal{V}_{kl}^{(n)}$. In this subsection, we exploit the equation (22) and re-write $c_n\{2q\}$ in terms of $\mathcal{E}_{kl}^{(n)}$.

In order to find general form of $c_n\{2q\}$ in terms of $\hat{\mathcal{E}}_{kl}^{(n)}$, the following remarks must be considered.

- In Elliptic-Power distribution, one can check that for $n = 2$ it is a good approximation to consider $\mathcal{E}_2^{(n)} \equiv \mathcal{E}_{02}^{(n)} \simeq \mathcal{E}_{20}^{(n)}$. It turns out that for $n = 3$, this relation becomes exact.

- An explicit calculation shows that terms $\hat{\mathcal{E}}_{10}^{2k-2}\hat{\mathcal{E}}_{02}$ has the same coefficient as $\hat{\mathcal{E}}_{10}^{2k-2}\hat{\mathcal{E}}_{20}$ but with oppo-

site sign[9]. Also for the Elliptic-Power distributions, the cumulant $\hat{\mathcal{E}}_{11}^{(n)}=0$.

Using all the above considerations together with (18), one finds

$$\begin{aligned}\frac{c_n\{2k\}}{\alpha^{2k}\mathcal{E}_2^k} \simeq & \#_1\hat{\mathcal{E}}_{10}^{2k}+\hat{\mathcal{E}}_{10}^{2k-3}(\#_2\hat{\mathcal{E}}_{30}+\#_3\hat{\mathcal{E}}_{12}+\cdots)\\ & +\#_4\hat{\mathcal{E}}_{10}^{2k-q}\hat{\mathcal{E}}_{q,0}+\cdots+\#_l\hat{\mathcal{E}}_{2k-q',q'}+\cdots .\end{aligned} \tag{23}$$

Recall that due to the symmetries of Elliptic-Power distribution, all the standardized cumulants $\hat{\mathcal{E}}^{(2)}_{k,2q+1}$ are zero for $n=2$ while for $n=3$, the only non-zero cumulants are $\hat{\mathcal{E}}^{(3)}_{2k,2q}$.

In Fig.5, we have compared a number of cumulants extracted from Elliptic-Power distribution with each other. Obviously, the non-vanishing $\hat{\mathcal{E}}_{pq}$ for $p+q\geq 3$ indicates that the Elliptic-Power distribution is not Gaussian. So we may describe the Elliptic-Power distribution by the two dimensional Gram-Charlier A series. Let us briefly explain how it works.

A general two dimensional distribution $\mathcal{P}(\xi_x,\xi_y)$ can be written as (Appendix B)

$$\mathcal{P}(\xi_x,\xi_y)\simeq\frac{1+\mathcal{H}}{2\pi\sqrt{\mathcal{A}_{20}\mathcal{A}_{02}}}e^{-\frac{(\xi_x-\mathcal{A}_{10})^2}{2\mathcal{A}_{20}}-\frac{(\xi_y-\mathcal{A}_{01})^2}{2\mathcal{A}_{02}}} \tag{24}$$

where

$$\mathcal{H}=\sum_{\substack{m=n=1,\\ m+n\geq 3}}\frac{\hat{\mathcal{A}}_{mn}}{m!n!}He_n(\frac{\xi_x-\mathcal{A}_{10}}{\sqrt{\mathcal{A}_{20}}})He_m(\frac{\xi_y-\mathcal{A}_{01}}{\sqrt{\mathcal{A}_{02}}}) \tag{25}$$

In the above, He_n is the Hermit polynomial. The equation (24) is the two dimensional Gram-Charlier A series. For Gaussian distributions, $\mathcal{H}=0$ while to each non-Gaussian distribution, a certain set of coefficients $\hat{\mathcal{A}}_{mn}$ have non-zero values. In the following, we study $\hat{\mathcal{A}}_{mn}$ associated with Elliptic-Power distribution by replacing $\hat{\mathcal{A}}_{mn}$ with $\hat{\mathcal{E}}_{mn}$ in (24).

As can be seen in Fig.5, typically by increasing $p+q$ the value of $\hat{\mathcal{E}}_{pq}$ increases. It has been checked that the increase rate of $\hat{\mathcal{E}}_{pq}$ is smaller than that of $p!q!$. As a result, the coefficients of successive terms in the expansion (25) are decreasing.

In the next two subsections, we will study the truncation of the expansion (23) for $n=2$ and $n=3$ separately. As an important requirement, we have to know the order of magnitude of terms in (23). This remark will be studied in the following.

In $n=2$, the non-zero value for $\hat{\mathcal{E}}_{10}$ comes from the ellipticity of the initial condition in non-central collisions. Its value is relatively larger than the cumulants originated from the event-by-event fluctuations (see Fig. 3). In this case, we expect the terms to be ordered with decreasing power of $\hat{\mathcal{E}}_{10}$ [10]. The leading order (LO) comes from $\hat{\mathcal{E}}_{10}^{2k}$ and the next to leading order (NLO) is $\hat{\mathcal{E}}_{10}^{2k-3}(\#_1\hat{\mathcal{E}}_{30}+\#_2\hat{\mathcal{E}}_{12}+\cdots)$.

For $n=3$, the situation is reversed. In this case, all the non-zero cumulants are coming from the event-by-event fluctuations and $\hat{\mathcal{E}}_{10}$ is zero due to the symmetry. As we observed in Fig.5(b), we expect the leading term of $c_3\{2k\}$ to be $\hat{\mathcal{E}}_{pq}$ with $p+q=2k$. Let us note that although $\hat{\mathcal{E}}_{pq}$ with $p+q=2k$ has the main contribution to $c_3\{2k\}$, it does not seriously affect on the deviation of the distribution from Gaussianity.

B. Truncating $c_2\{2k\}$ Expansion

As we mentioned earlier, the distribution of ε_2 is not rotationally symmetric. We have also seen that it is skewed in the $\varepsilon_{2,x}$ direction (see Fig.1(a)). In what follows in this subsection, we argue that the other higher order cumulants of ε_2 distribution can not be extracted from $c_2\{2k\}$ truncation.

Let us emphasis that, we only keep terms with decreasing power of $\hat{\mathcal{E}}_{10}^{(2)}$ in $c_2\{2k\}$ expansion. In order to get fairly accurate result up to 60% centrality for $c_2\{2k\}$, $k=2,3,4$ (see Fig.6), we have to use the following truncations

$$\frac{c_2\{2\}}{\alpha_2^2\mathcal{E}_2}\simeq\hat{\mathcal{E}}_{10}^2+2 \tag{26}$$

$$\begin{aligned}\frac{c_2\{4\}}{\alpha_2^4\mathcal{E}_2^2}\simeq & -\hat{\mathcal{E}}_{10}^4+4\hat{\mathcal{E}}_{10}\left(\hat{\mathcal{E}}_{30}+\hat{\mathcal{E}}_{12}\right)\\ & +\hat{\mathcal{E}}_{40}+\hat{\mathcal{E}}_{22}+\hat{\mathcal{E}}_{04}\end{aligned} \tag{27}$$

$$\begin{aligned}\frac{c_2\{6\}}{\alpha_2^6\mathcal{E}_2^3}\simeq & 4\hat{\mathcal{E}}_{10}^6-8\hat{\mathcal{E}}_{10}^3\left(2\hat{\mathcal{E}}_{30}+3\hat{\mathcal{E}}_{12}\right)\\ & +6\hat{\mathcal{E}}_{10}^2(\hat{\mathcal{E}}_{40}-\hat{\mathcal{E}}_{04})\\ & +6\hat{\mathcal{E}}_{10}\left(\hat{\mathcal{E}}_{50}+2\hat{\mathcal{E}}_{32}+\hat{\mathcal{E}}_{14}\right)\end{aligned} \tag{28}$$

$$\begin{aligned}\frac{c_2\{8\}}{\alpha_2^8\mathcal{E}_2^4}\simeq & -33\hat{\mathcal{E}}_{10}^8+24\hat{\mathcal{E}}_{10}^5\left(7\hat{\mathcal{E}}_{30}+11\hat{\mathcal{E}}_{12}\right)\\ & -\hat{\mathcal{E}}_{10}^4(62\hat{\mathcal{E}}_{40}+12\hat{\mathcal{E}}_{22}-66\hat{\mathcal{E}}_{04})\\ & -8\hat{\mathcal{E}}_{10}^3(5\hat{\mathcal{E}}_{50}+14\hat{\mathcal{E}}_{32}-9\hat{\mathcal{E}}_{14})\\ & -12\hat{\mathcal{E}}_{10}^2(\hat{\mathcal{E}}_{60}+\hat{\mathcal{E}}_{42}-14\hat{\mathcal{E}}_{30}^2\\ & \qquad -44\hat{\mathcal{E}}_{30}\hat{\mathcal{E}}_{12}-\hat{\mathcal{E}}_{24}-30\hat{\mathcal{E}}_{12}^2-\hat{\mathcal{E}}_{06}).\end{aligned} \tag{29}$$

In Fig.6, we did not plot $c_2\{2\}$ because the relation (26) is almost exact with the only approximation $\mathcal{E}_{20}\simeq\mathcal{E}_{02}$. In the same figure, by moving from $c_2\{4\}$ to $c_2\{8\}$ more terms are needed to find a good approximation compare to the exact relation.

[9] We checked it for $k=2,3,4,5,6$

[10] As we explained earlier in the current subsection, $\hat{\mathcal{E}}_{pq}$ increases by increasing $p+q$. The argument we used here may be no longer valid for $c_2\{2k\}$, $k>4$, while, it is reliable for $c_2\{2\}$, $c_2\{4\}$, $c_2\{6\}$ and $c_2\{8\}$ as we will see in the next subsection.

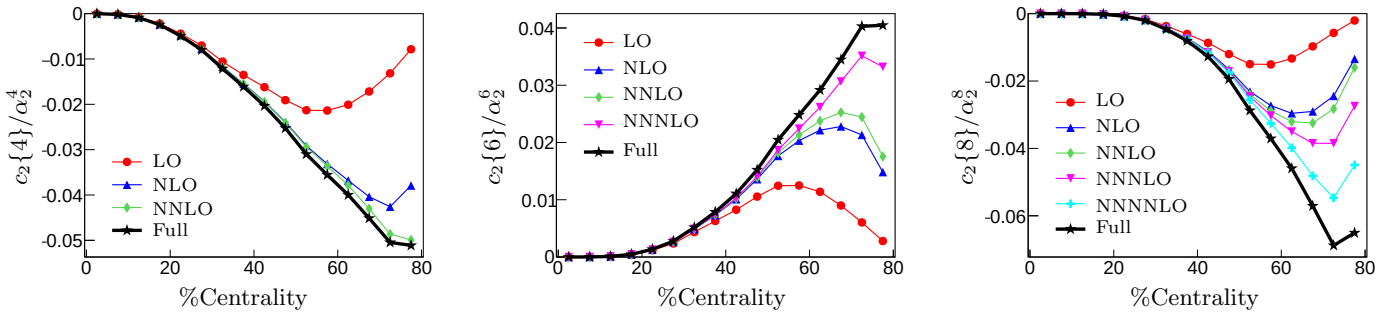

FIG. 6. (Color online) Comparing different values of $c_2\{4\}$, $c_2\{6\}$ and $c_2\{8\}$ in the standardized cumulant expansion truncation.

These observations are in agreement with the results of Ref.[13]. In [13], only the NLO terms, i.e. the contributions in the first line in each of equations (26) to (29), have been considered. By use of this approximation, the authors of [13], computed $\mathcal{E}_{30}^{(2)}$, considering $c_2\{2\}$, $c_2\{4\}$ and $c_2\{6\}$ [11]. Their results are in agreement with experimental data. It is worth mentioning that the approximation they used is obtained by studying a full hydrodynamic simulation.

Note that if we are interested in finding cumulants beyond skewness, $c_2\{8\}$ is needed to be taken into account. However, as can be seen from Fig.6, going from NLO to NNLO does not improve the accuracy of $c_2\{6\}$ and $c_2\{8\}$ remarkably. In other words, it would not be easy to find the standardized cumulants beyond the skewness for the elliptic flow distribution.

C. Truncating $c_3\{2k\}$ Expansion

Unlike the ε_2 distribution case, for ε_3 the distribution is rotationally symmetric in ($\varepsilon_{3,x}$-$\varepsilon_{3,y}$) plane (see Fig.1(b) and Eq.(5)). As a result, ε_3 distribution is not skewed, however, it can have a non-zero kurtosis in the radial direction. In what follows, we calculate a number of non-zero cumulants, including kurtosis, in the radial direction.

Considering (23) for $c_3\{2k\}$ expansion and the previously mentioned properties of $\mathcal{E}_{pq}^{(3)}$ for Elliptic-Power distribution, one finds

$$\mathcal{K}_2 \equiv \frac{c_3\{2\}}{\alpha_2^2} = \mathcal{E}_{20} + \mathcal{E}_{02}, \tag{30}$$

$$\mathcal{K}_4 \equiv \frac{c_3\{4\}}{\alpha_2^4} = \mathcal{E}_{40} + 2\mathcal{E}_{22} + \mathcal{E}_{04}, \tag{31}$$

$$\mathcal{K}_6 \equiv \frac{c_3\{6\}}{\alpha_2^6} = \mathcal{E}_{60} + 3\mathcal{E}_{42} + 3\mathcal{E}_{24} + \mathcal{E}_{06}. \tag{32}$$

[11] The approximate $c_2\{2\}$, $c_2\{4\}$ and $c_2\{6\}$ used in [13], have been depicted by blue curves in Fig.6.

Note that the relations (30)-(32) are exact, by this we mean that we have not used any truncation when deriving them. However, for distributions obtained from more realistic models (e.g. MC-Glauber), the above relations are truncations of expansion (23) and so approximately true.

In order to show the relation between the cumulants in the radial direction and $\mathcal{K}_q$, let us use the polar coordinate $\varepsilon_{3,x} = \varepsilon_3 \cos\varphi$ and $\varepsilon_{3,y} = \varepsilon_3 \sin\varphi$. Doing so, we obtain[12],

$$\langle \varepsilon_{3,x}^m \varepsilon_{3,y}^n \rangle_{EP} = \langle \varepsilon_3^{m+n} \rangle_P \int \frac{d\varphi}{2\pi} \cos^m\varphi \sin^n\varphi. \tag{33}$$

In this equation, the average in the left hand side has been taken by the distribution function (4) while for the average in the right hand side, the distribution (5) has been used. In general, for any rotationally symmetric distribution, the averaging in the azimuthal integration is factorized and the moments with either odd m or odd n vanish.

In the right hand side of the equations (30) to (32), the cumulants $\mathcal{E}_{pq}^{(3)}$ have been written in terms of moments $\langle \varepsilon_{3,x}^m \varepsilon_{3,y}^n \rangle_{EP}$. One can substitute (33) into (30) to (32) to find $\mathcal{K}_n$ in terms of moment $\langle \varepsilon_3^q \rangle_P$. As an example

$$\mathcal{K}_2 = \langle \varepsilon_3^2 \rangle_P,$$
$$\mathcal{K}_4 = \langle \varepsilon_3^4 \rangle_P - 3\langle \varepsilon_3^2 \rangle_P^2.$$

On the other hand, the cumulants κ_2 and κ_4 (introduced in section III A) of the one dimensional power distribution (5) is given by

$$\kappa_2 = \langle \varepsilon_3^2 \rangle_P - \langle \varepsilon_3 \rangle_P^2,$$
$$\kappa_4 = \langle \varepsilon_3^4 \rangle_P - 4\langle \varepsilon_3^3 \rangle_P \langle \varepsilon_3 \rangle_P - 3\langle \varepsilon_3^2 \rangle_P^2 + 12\langle \varepsilon_3^2 \rangle_P \langle \varepsilon_3 \rangle_P^2 - 6\langle \varepsilon_3 \rangle_P^4.$$

In fact, $\mathcal{K}_n$ coincides with κ_n if the moments $\langle \varepsilon_3^{2q+1} \rangle$ are removed. This actually happens for every rotationally

[12] In this subsection, in order to clearly distinguish between averaging over Elliptic-Power and Power distribution, we use the subscripts EP and P respectively.

symmetric distribution due to the φ integral in (33). As a result, the standardized cumulants of such distribution may be written in terms of $\mathcal{K}_q$ as follows,

$$\Gamma_{q-2} = \frac{\mathcal{K}_q}{\mathcal{K}_2^{q/2}}. \tag{34}$$

For instance, Γ_2 is the kurtosis. In this case, the skewness, Γ_1, is zero because $\mathcal{K}_3 = 0$.

Rotational symmetry suggests to integrate over the azimuthal angle in (24). To do so, we change the variable (ξ_x, ξ_y) to (ξ_r, ξ_ϕ) with $\xi_r = (\xi_x^2 + \xi_y^2)^{1/2}$ and $\xi_\phi = \text{atan2}(\xi_y/\xi_x)$. Using (20) and after some cumbersome calculations, one obtains (see Appendix B for more details),

$$p(v_3) = \left[1 + \Gamma_2 \mathcal{Q}_4(\frac{v_3}{v_3\{2\}}) + \Gamma_4 \mathcal{Q}_6(\frac{v_3}{v_3\{2\}}) + \cdots\right] \times \frac{2v_3}{v_3^2\{2\}} \exp\left[-\frac{v_3^2}{v_3^2\{2\}}\right] \tag{35}$$

where

$$\Gamma_2 = (\hat{\mathcal{V}}_{40} + 2\hat{\mathcal{V}}_{22} + \hat{\mathcal{V}}_{04})/4, \tag{36}$$

$$\Gamma_4 = (\hat{\mathcal{V}}_{60} + 3\hat{\mathcal{V}}_{42} + 3\hat{\mathcal{V}}_{24} + \hat{\mathcal{V}}_{06})/8, \tag{37}$$

and

$$\mathcal{Q}_4(\xi) = \frac{1}{4}\left[\xi^4 - 4\,\xi^2 + 2\right], \tag{38}$$

$$\mathcal{Q}_6(\xi) = \frac{1}{36}\left[\xi^6 - 9\,\xi^4 + 18\,\xi^2 - 6\right]. \tag{39}$$

By using equation (21) together with equations (30) to (32) we find

$$\Gamma_2 = -\left(\frac{v_3\{4\}}{v_3\{2\}}\right)^4, \tag{40}$$

$$\Gamma_4 = 4\left(\frac{v_3\{6\}}{v_3\{2\}}\right)^6. \tag{41}$$

We call the distribution (35) *Radial-Gram-Charlier* (RGC) distribution. Here, the random variable is v_3 while $v_3\{2\}$, Γ_2 and Γ_4 are constants that can be obtained by fitting process. Note that if we set $\Gamma_2 = \Gamma_4 = 0$ then the Gaussian distribution is found.

In this section, we studied the reasonable truncation of $2q$-particle correlation cumulant expansion by exploiting a semi-analytical model. More importantly, we found a new distribution $p(v_3)$ which describes the leading deviation of v_3 distribution from Gaussian distribution, with two parameters, namely Γ_2 and Γ_4. The results of model we used in this section (Elliptic-Power together linear hydro.) are not too reliable to be compared with the experimental data. For this reason, in the next section, we use a more realistic model, i.e. iEBE-VISHNU event generator together with MC-Glauber model. To compare with experimental data, we then apply the truncations obtained in current section to the mentioned model, using also the RGC distribution.

V. MC-GLAUBER MODEL AND BEYOND HYDRODYNAMIC LINEAR RESPONSE

The skewness of v_2 distribution has been calculated in [13] by using the viscous relativistic hydrodynamical code V-USPHYDRO [34–36]. While in the same reference, the skewness has been also found from experimental data, nothing has been mentioned about v_3 distribution there. In the current section, we focus on finding the standardized cumulants of v_3 distribution.

Here, we use the heavy ion collision event generator, iEBE-VISHNU [16] to study the evolution of the initial state generated by MC-Glauber model (implemented in iEBE-VISHNU). After generating the initial condition, we let it evolve through a 2+1 dimensional viscose hydrodynamic model based on the causal Israel-Stewart formalism. At the end of the hydrodynamic evolution, each fluid element on the freeze-out hypersurface converts into the particle distribution by Cooper-Frye formula. Then the particle distribution is used to simulate the next step which is the hadronic gas phase. Indeed, it is done by Ultrarelativistic Quantum Molecular Dynamics (UrQMD) transport model [37]. The evolution goes on until neither any interaction exists in the medium nor unstable hadrons remain to decay.

We study Pb-Pb collisions with center of mass energy $\sqrt{s} = 2.76\,\text{TeV}$. We divide the centralities between 0-80% into 16 equal bins and for each bin we generate 7000 events in the range of 0-40% centralities and 14000 events in the range of 45-80%. In the MC-Glauber, we set the wounded nucleon/binary collision mixing parameter to be 0.118 and in the hydrodynamic evoluton we choose the shear viscosity over entropy density, η/s, to be 0.08. In this simulation, the reaction plane angle ψ_{RP} has been taken to be equal to zero for all events.

After generating the heavy ion collision events, we can find the distribution of $p(v_n)$ for each centrality bin. The ATLAS collaboration also reported this probability distribution in [38]. Consequently, in addition to relation (40), we can find Γ_2 (and Γ_6) by fitting the RGC-distribution with the ATLAS results. In Fig.7, we have plotted this distribution for 50-55% centrality and fitted with the ATLAS experimental data by either a Gaussian distribution (red dashed curve) and a RGC distribution (35) (red solid curve). As one expects, the Monte-Carlo simulation has a good agreement with data. More importantly, the result obtained from the RGC distribution indicates a better fit with that of Gaussian distribution. Similar to RGC distribution, the power distribution fits with data accurately[12]. However, from the RGC distribution fit, one can find Γ_2 and Γ_4 as well [13].

[13] Due to the small numerical factor $\frac{1}{36}$ in (39), the effect of the Γ_4 on the distribution is small and therefore we need lots of events to find a reasonable value via fitting. We checked that by setting $\Gamma_4 = 0$, the result obtained for Γ_2 is not changed drastically.

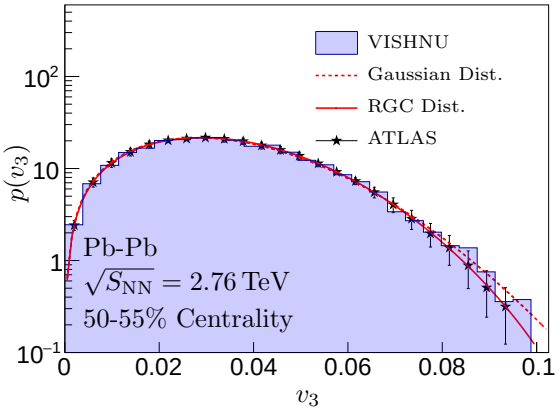

FIG. 7. (Color online) Comparing the experimental data of ATLAS for $p(v_3)$ with MC-Glauber, Gaussian distribution and RGC distribution. The χ^2 for Gaussian distribution fit is ~ 3.36 and for RGC distribution is ~ 0.17. The ATLAS results have been obtained from $7\mu b^{-1}$ data [38].

From simulation, we can also find the distribution of $p(v_{3,x}v_{3,y})$ for each centrality bin and consequently determine the standardized cumulants $\hat{\mathcal{V}}^{(3)}_{pq}$. The results have been plotted by black dots in Fig.3 and Fig.4. As can be seen, $\hat{\mathcal{V}}^{(3)}_{pq}$ and $\hat{\mathcal{E}}^{(3)}_{pq}$ have more agreements with each other in lower centralities. In higher centralities $\hat{\mathcal{E}}^{(3)}_{pq}$ deviates from $\hat{\mathcal{V}}^{(3)}_{pq}$ significantly. This is due to presence of more fluctuations in higher centralities.

Now we can obtain the kurtosis from both the simulation and experiment: we use (40) with $v_3\{2\}$ and $v_3\{4\}$ obtaining from experimental data. We also use (34) together with the equations (30) and (31) from simulation. The resultant kurtosis has been depicted by black dots in Fig.8(a). Using (40), in the same figure, the kurtosis obtained directly from ATLAS data has been plotted by the shaded blue region. The shaded gray region is the kurtosis obtained by fitting the RGC distribution with $p(v_3)$ generated by iEBE-VISHNU. As can be seen, it is in good agreement with the kurtosis obtained directly from simulation; this means that RGC-distribution works well.

Considering the Fig.8(a), for centralities between 40% to 60% there is a good agreement between iEBE-VISHNU simulation and ATLAS data. However, it is not true for smaller centralities. In fact, we observe a wrong sign in smaller centralities. It is worth mentioning that we are using the data generated by iEBE-VIISHNU where the quantity $\hat{\mathcal{V}}^{(2)}_{30}$ plotted in Fig.3(b) is in agreement with the same quantity obtained from hydrodynamic code V-USPHYDRO [34–36] (Fig.2 in [13]). Moreover the quantity $(-\Gamma_2)^{1/4}$ plotted in the recent work [15] behaves similar to what we showed in Fig.8(a). At the moment, the origin of the discrepancy between the data and simulations in the centralities below the 40% is not known to us.

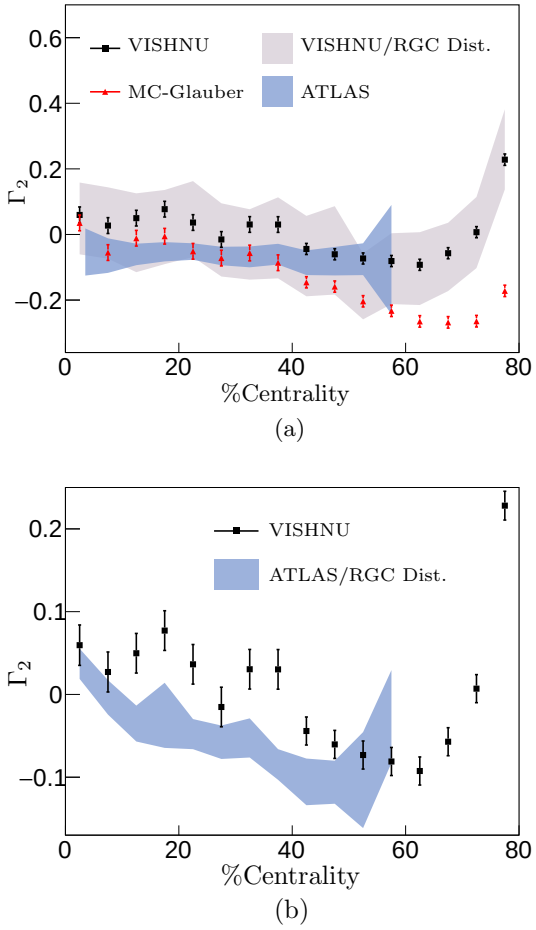

FIG. 8. (Color online) The kurtosis with respect to centrality obtained from Elliptic-Power distribution together with hydrodynamic linear response, iEBE-VISHNU and ATLAS data. In (a), the red dots obtained from MC-Glauber and black dots are related to their hydrodynamic evolution. We use (30) to (32) to calculate them. The shaded gray region is the kurtosis of v_3 distribution obtained by fitting (35) to output of the simulation. The blue shaded region is the kurtosis calculated from ATLAS data [9] by using (40). The plot in (b), is the zoomed in of plot (a). The black dots are same as before, but, the blue shaded region is the kurtosis obtained by fitting (35) to ATLAS results for $p(v_3)$ [38].

In Fig.8(b), we obtain the Γ_2 by fitting the RGC-distribution with $p(v_3)$ reported by ATLAS collaboration [38] (see Fig.7). Note that this is an independent way of finding the kurtosis from experimental data, in comparison with Fig.8(a). The Γ_2 obtained with this procedure has relatively small error bars and as can be seen, it has positive sign for very small centralities. Except some fluctuating bins, there is more agreement between the experimental data and simulations than the procedure in the previous paragraph. The fluctuating bins in 10% to 40% centralities can be seen also in $\hat{\mathcal{V}}^{(3)}_{04}$ (Fig.4(b)).

The source of them may be is due to the statistical fluctuations.

VI. CONCLUSION

In this work, we have studied the standardized cumulants of v_2 and v_3 distribution. We found that in v_2 distribution, it is difficult to find the standardized cumulants beyond skewness experimentally. However in v_3, the higher order standardized cumulants can be observed in the experiment. Specifically, the non-zero kurtosis and sixth order standardized cumulant are responsible for non-zero values of $c_3\{4\}$ and $c_3\{6\}$ respectively. We have found a new distribution $p(v_3)$ with kurtosis and sixth order standardized cumulant as its free parameters. It is obtained by integrating over the azimuthal angle of the two dimensional Gram-Charlier A series. We have shown that compared to the Gaussian distribution, it suitably fits the experimental data. We have also compared the kurtosis obtained from experiment with that of computed by simulation. We have calculated the kurtosis from experimental data by applying two different methods: first by using $-(v_3\{4\}/v_3\{2\})^4$ and second by fitting radial Gram-Charlier distribution with the $p(v_3)$ obtained from experiment.

Here we have derived the RGC distribution for third order flow harmonic. However, it would be interesting to generalize RGC to the case of other flow harmonics. If it is fulfilled, it could be an alternative for either Elliptic-Power and Bessel-Gaussian distribution [39].

ACKNOWLEDGMENTS

We would like to thank Prof. Mohsen Alishahiha for encouragements and supporting the Larak-Particle-Pheno group. We would also like to thank M. Mohammadi Najafaabdi for reading the paper thoroughly and giving useful comments. We thank to U. A. Wiedemann for discussions and useful comments on manuscript during our visit to CERN. We would like to thank J. Ollitrault, G. Giacalone and J. Noronha-Hostler for discussions via exchanging several emails and special thanks to J. Ollitrault and G. Giacalone for warm hospitality in the short meeting in CEA Saclay and comments on manuscript. We thank A. Akhavan for useful discussion. We would like to thank B. Safarzadeh, M. Naseri and H. Behnamian. We thank to participants of "IPM Workshop on Particle Physics Phenomenology". We would like to thank the CERN TH Unit for hospitality during the final steps of this work.

Appendix A: Analytical Relations for Elliptic-Power Moments

The solution of integral (10) for both even and odd values of m is given by

$$I_{2k}(q,\alpha,\beta) = \sqrt{\pi}\Gamma\left(k+\frac{1}{2}\right)\Gamma(\alpha+1) \times {}_3\tilde{F}_2(k+\frac{1}{2},\frac{\beta+1}{2},\frac{\beta}{2};\frac{1}{2},\alpha+k+\frac{3}{2};\varepsilon_0^2), \tag{A1}$$

$$I_{2k+1}(q,\alpha,\beta) = \frac{\varepsilon_0\beta\sqrt{\pi}}{2}\Gamma\left(k+\frac{3}{2}\right)\Gamma(\alpha+1) \times {}_3\tilde{F}_2(k+\frac{3}{2},\frac{\beta+1}{2},\frac{\beta+2}{2};\frac{3}{2},\alpha+k+\frac{5}{2};\varepsilon_0^2), \tag{A2}$$

where ${}_3\tilde{F}_2$ is the regularized hypergeometric function. Specifically,

$$I_{2k}(0,\alpha-1,0) = \frac{\Gamma(\alpha)\Gamma(k+1/2)}{\Gamma(\alpha+k+1/2)}, \tag{A3a}$$

$$I_{2k+1}(0,\alpha-1,0) = 0. \tag{A3b}$$

Using these relations, the moments of the Elliptic-Power distribution can be found as the following

$$\langle \varepsilon_{n,x}^{k}\varepsilon_{n,y}^{2l+1}\rangle = 0, \tag{A4}$$

$$\langle \varepsilon_{n,x}^{2k}\varepsilon_{n,y}^{2l}\rangle = (X_{2k})\ {}_3\tilde{F}_2(k+\frac{1}{2},\alpha+1,\alpha+\frac{1}{2};\frac{1}{2},1+l+k+\alpha;\varepsilon_0^2), \tag{A5}$$

$$\langle \varepsilon_{n,x}^{2k+1}\varepsilon_{n,y}^{2l}\rangle = \varepsilon_0(X_{2k+1})\ {}_3\tilde{F}_2(k+\frac{3}{2},\alpha+1,\alpha+\frac{3}{2};\frac{3}{2},2+l+k+\alpha;\varepsilon_0^2), \tag{A6}$$

where

$$X_{2k} = \frac{\alpha}{\sqrt{\pi}}\left(1-\varepsilon_0^2\right)^{\alpha+\frac{1}{2}}\Gamma(\alpha)\Gamma(k+1/2)\Gamma(l+1/2), \tag{A7}$$

$$X_{2k+1} = \frac{\alpha(1+2\alpha)}{2\sqrt{\pi}}\left(1-\varepsilon_0^2\right)^{\alpha+\frac{1}{2}} \times\Gamma(\alpha)\Gamma(k+1/2)\Gamma(l+1/2). \tag{A8}$$

Note that for the case $\varepsilon_0 = 0$, the only non-zero moments are as $\langle \varepsilon_{n,x}^{2k}\varepsilon_{n,y}^{2l}\rangle$.

Appendix B: Radial-Gram-Charlier Distribution

1. 2D Gram-Charlier A Series

The expansion of a one-dimensional distribution in terms of its cumulants is well-known (see for instance the textbook [28]). In this Appendix, we review the generalization of such distribution to the two dimensions. Let

us start with (7) and consider $\lambda_x \to i\lambda_x$ and $\lambda_y \to i\lambda_y$. So we can write the equation (7) as it follows

$$\int d\xi_x d\xi_y \mathcal{P}(\xi_x,\xi_y) e^{i(\lambda_x\xi_x+\lambda_y\xi_y)} = \mathcal{P}(\lambda_x,\lambda_y) = \exp\left[\sum_{m,n=0} \frac{(i\,\lambda_x)^m (i\,\lambda_y)^n}{m!n!}\mathcal{A}_{mn}\right]. \tag{B1}$$

Note that by $\mathcal{P}(\lambda_x,\lambda_y)$ in the second line, we mean the Fourier transformation of $\mathcal{P}(\xi_x,\xi_y)$. For the special case where $\mathcal{P}(\xi_x,\xi_y)$ is the 2D normal distribution

$$N(\xi_x,\xi_y) = \frac{1}{2\pi\sigma_x\sigma_y} e^{-\frac{(\xi_x-\mu_x)^2}{2\sigma_x^2}-\frac{(\xi_y-\mu_y)^2}{2\sigma_y^2}} \tag{B2}$$

we have

$$N(\lambda_x,\lambda_y) = \exp\left[\sum_{m,n=0} \frac{(i\,\lambda_x)^m (i\,\lambda_y)^n}{m!n!}\mathcal{N}_{mn}\right] \tag{B3}$$

with the only non-zero cumulants being $\mathcal{N}_{10}=\mu_x, \mathcal{N}_{01}=\mu_y$, $\mathcal{N}_{20}=\sigma_x^2$ and $\mathcal{N}_{02}=\sigma_y^2$. Let us consider the first cumulants of the distribution $\mathcal{P}(\xi_x,\xi_y)$ are $\mathcal{A}_{10}=\mathcal{N}_{10}$, $\mathcal{A}_{01}=\mathcal{N}_{01}$, $\mathcal{A}_{20}=\mathcal{N}_{20}$ and $\mathcal{A}_{02}=\mathcal{N}_{02}$. By combining the equations (B1) and (B3) with each other, we can write a general distribution as

$$\mathcal{P}(\lambda_x,\lambda_y) = \exp\left[\sum_{\substack{m=n=1,\\ m+n\geq 3}} \frac{(i\,\lambda_x)^m (i\,\lambda_y)^n}{m!n!}\mathcal{A}_{mn}\right] N(\lambda_x,\lambda_y). \tag{B4}$$

with its Fourier transformed being as

$$\mathcal{P}(\xi_x,\xi_y) = \exp\left[\sum_{\substack{m=n=1,\\ m+n\geq 3}} \frac{(-1)^{m+n}}{m!n!}\mathcal{A}_{mn}\frac{\partial^{m+n}}{\partial\xi_x^n\partial\xi_y^m}\right] N(\xi_x,\xi_y). \tag{B5}$$

In order to compute the derivatives in the exponential in this equation, let us remind the Hermite polynomial defined through

$$(-1)^m \frac{\partial^m}{\partial\xi_x^m} e^{-\frac{\xi_x^2}{2}} = He_m(\xi_x) e^{-\frac{\xi_x^2}{2}}. \tag{B6}$$

Using (B2), we immediately find

$$(-1)^{m+n}\frac{\partial^{m+n}}{\partial\xi_x^n\partial\xi_y^m} N(\xi_x,\xi_y) = \frac{1}{\sigma_x^m\sigma_y^n} He_m(\frac{\xi_x-\mu_x}{\sigma_x}) He_n(\frac{\xi_y-\mu_y}{\sigma_y}) N(\xi_x,\xi_y). \tag{B7}$$

Now by considering the small deviation from Gaussian, we can expand the exponential and keep the linear terms in (B5). This simply gives (24).

2. Integration Over azimuthal Angle

In this Appendix we consider a generic 2D rotationally (with respect to origin) symmetric distribution and integrate over the azimuthal angle.

Let us firstly change the variables (ξ_x,ξ_y) to (ξ_r,ξ_ϕ) with $\xi_r = \sqrt{\xi_x^2+\xi_y^2}$ and $\xi_\phi = \text{atan2}(\xi_y/\xi_x)$. In this special case, we have $\mu_x=\mu_y=0$ and $\sigma\equiv\sigma_x=\sigma_y$. By using the definition of Hermite polynomials we find,

$$He_n(\xi_x)He_m(\xi_y) = (-1)^{m+n} e^{\frac{\xi_r^2}{2}} \frac{\partial^{m+n}}{\partial\xi_x^n\partial\xi_y^m} e^{-\frac{\xi_r^2}{2}}. \tag{B8}$$

On the other hand, the multi-differentiation of an arbitrary function $f(\xi_r)$ with respect to (ξ_x,ξ_y) has the following form in the polar coordinate

$$\frac{\partial^{m+n}}{\partial\xi_x^n\partial\xi_y^m} f(\xi_r) = \left(\sum_{i=1}^{m+n} g_i^{mn}(\xi_\phi)\frac{d^i}{d\xi_r^i}\right) f(\xi_r), \tag{B9}$$

with some of the coefficient functions being as

$$g_1^{20} = \frac{\sin^2(\xi_\phi)}{r}, \qquad g_2^{02} = \cos^2(\xi_\phi), \tag{B10}$$

$$g_1^{11} = -\frac{\sin(\xi_\phi)\cos(\xi_\phi)}{r}, \; g_2^{11} = \sin(\xi_\phi)\cos(\xi_\phi), \tag{B11}$$

$$g_1^{02} = \frac{\cos^2(\xi_\phi)}{r}, \qquad g_2^{02} = \sin^2(\xi_\phi). \tag{B12}$$

Using (B8) and (B9), we have

$$He_n(\xi_x)He_m(\xi_y) = (-1)^{m+n}\sum_{i=1}^{m+n}(-1)^i g_i^{mn}(\xi_\phi) He_i(\xi_r). \tag{B13}$$

Let us define the following integral,

$$J_{mn}(\frac{\xi_r}{\sigma}) = \int_0^{2\pi} d\xi_\phi He_n(\frac{\xi_x}{\sigma}) He_m(\frac{\xi_y}{\sigma}). \tag{B14}$$

A few first terms of $J_{mn}(\xi_r)$ are listed in the following

$$J_{20}(\xi_r) = \pi\xi_r^2 - 2\pi, \tag{B15}$$

$$J_{40}(\xi_r) = \frac{3\pi}{4}\xi_r^4 - 6\pi\xi_r^2 + 6\pi, \tag{B16}$$

$$J_{22}(\xi_r) = \frac{1}{3}J_{40}(\xi_r), \tag{B17}$$

$$J_{60}(\xi_r) = \frac{5\pi}{8}\xi_r^6 - \frac{45\pi}{4}\xi_r^4 + 45\pi\xi_r^2 - 30\pi, \tag{B18}$$

$$J_{42}(\xi_r) = \frac{1}{5}J_{60}(\xi_r). \tag{B19}$$

It is worth mentioning that J_{mn} is non-zero only for $n=2p$ and $m=2q$. It can be also shown that $J_{mn}(\xi_r) = J_{nm}(\xi_r)$.

Consequently the radial distribution in (24) reads

$$\int d\xi_r p(\xi_r) = \int \frac{\xi_r d\xi_r}{2\pi\mathcal{A}_2} e^{-\frac{\xi_r^2}{2\mathcal{A}_2}} \int d\xi_\phi \, (1+\mathcal{H}) = \int \frac{\xi_r d\xi_r}{2\pi\mathcal{A}_2} e^{-\frac{\xi_r^2}{2\mathcal{A}_2}} \left[2\pi + \sum_{\substack{m=n=1,\\ m+n\geq 3}} \frac{J_{mn}(\frac{\xi_r}{\sigma})(-1)^{m+n}}{m!n!} \hat{\mathcal{A}}_{mn} \right] \tag{B20}$$

where by using equations (B16) to (B19) together with the equations (30) to (32), one reaches to (35). Let us recall that $\mathcal{A}_2 \equiv \mathcal{A}_{20} = \mathcal{A}_{02}$, $\mathcal{A}_{10} = \mu_x$ and $\mathcal{A}_{01} = \mu_y$. We have also $\xi_r = v_3$ and $2\sigma^2 = v_3^2\{2\}$ in (35).

[1] K. H. Ackermann *et al.* [STAR Collaboration], Phys. Rev. Lett. **86**, 402 (2001) doi:10.1103/PhysRevLett.86.402 [nucl-ex/0009011].

[2] K. Aamodt *et al.* [ALICE Collaboration], Phys. Rev. Lett. **105**, 252302 (2010) doi:10.1103/PhysRevLett.105.252302 [arXiv:1011.3914 [nucl-ex]].

[3] B. Alver and G. Roland, Phys. Rev. C **81**, 054905 (2010) Erratum: [Phys. Rev. C **82**, 039903 (2010)] doi:10.1103/PhysRevC.82.039903, 10.1103/PhysRevC.81.054905 [arXiv:1003.0194 [nucl-th]].

[4] A. Adare *et al.* [PHENIX Collaboration], Phys. Rev. Lett. **107**, 252301 (2011) doi:10.1103/PhysRevLett.107.252301 [arXiv:1105.3928 [nucl-ex]].

[5] P. Sorensen [STAR Collaboration], J. Phys. G **38**, 124029 (2011) doi:10.1088/0954-3899/38/12/124029 [arXiv:1110.0737 [nucl-ex]].

[6] K. Aamodt *et al.* [ALICE Collaboration], Phys. Rev. Lett. **107**, 032301 (2011) doi:10.1103/PhysRevLett.107.032301 [arXiv:1105.3865 [nucl-ex]].

[7] K. Aamodt *et al.* [ALICE Collaboration], Phys. Lett. B **708**, 249 (2012) doi:10.1016/j.physletb.2012.01.060 [arXiv:1109.2501 [nucl-ex]].

[8] W. Li [CMS Collaboration], J. Phys. G **38**, 124027 (2011) doi:10.1088/0954-3899/38/12/124027 [arXiv:1107.2452 [nucl-ex]].

[9] G. Aad *et al.* [ATLAS Collaboration], Eur. Phys. J. C **74**, no. 11, 3157 (2014) doi:10.1140/epjc/s10052-014-3157-z [arXiv:1408.4342 [hep-ex]].

[10] N. Borghini, P. M. Dinh and J. Y. Ollitrault, Phys. Rev. C **63**, 054906 (2001) doi:10.1103/PhysRevC.63.054906 [nucl-th/0007063].

[11] N. Borghini, P. M. Dinh and J. Y. Ollitrault, Phys. Rev. C **64**, 054901 (2001) doi:10.1103/PhysRevC.64.054901 [nucl-th/0105040].

[12] L. Yan, J. Y. Ollitrault and A. M. Poskanzer, Phys. Rev. C **90**, no. 2, 024903 (2014) [arXiv:1405.6595 [nucl-th]].

[13] G. Giacalone, L. Yan, J. Noronha-Hostler and J. Y. Ollitrault, arXiv:1608.01823 [nucl-th].

[14] R. S. Bhalerao, M. Luzum and J. Y. Ollitrault, Phys. Rev. C **84**, 054901 (2011) doi:10.1103/PhysRevC.84.054901 [arXiv:1107.5485 [nucl-th]].

[15] G. Giacalone, J. Noronha-Hostler and J. Y. Ollitrault, arXiv:1702.01730 [nucl-th].

[16] C. Shen, Z. Qiu, H. Song, J. Bernhard, S. Bass and U. Heinz, Comput. Phys. Commun. **199**, 61 (2016) doi:10.1016/j.cpc.2015.08.039 [arXiv:1409.8164 [nucl-th]].

[17] P. Danielewicz and M. Gyulassy, Phys. Lett. **129B**, 283 (1983).

[18] J. Y. Ollitrault, Phys. Rev. D **46**, 229 (1992).

[19] W. Broniowski, M. Rybczynski and P. Bozek, Comput. Phys. Commun. **180**, 69 (2009) doi:10.1016/j.cpc.2008.07.016 [arXiv:0710.5731 [nucl-th]].

[20] B. Alver, M. Baker, C. Loizides and P. Steinberg, arXiv:0805.4411 [nucl-ex].

[21] C. Loizides, J. Nagle and P. Steinberg, SoftwareX **1-2**, 13 (2015) doi:10.1016/j.softx.2015.05.001 [arXiv:1408.2549 [nucl-ex]].

[22] D. Kharzeev, E. Levin and M. Nardi, Phys. Rev. C **71**, 054903 (2005) doi:10.1103/PhysRevC.71.054903 [hep-ph/0111315].

[23] D. Kharzeev, E. Levin and M. Nardi, Nucl. Phys. A **747**, 609 (2005) doi:10.1016/j.nuclphysa.2004.10.018 [hep-ph/0408050].

[24] B. Schenke, P. Tribedy and R. Venugopalan, Phys. Rev. Lett. **108**, 252301 (2012) doi:10.1103/PhysRevLett.108.252301 [arXiv:1202.6646 [nucl-th]].

[25] D. Teaney and L. Yan, Phys. Rev. C **83**, 064904 (2011) [arXiv:1010.1876 [nucl-th]].

[26] S. Floerchinger and U. A. Wiedemann, Phys. Lett. B **728**, 407 (2014) doi:10.1016/j.physletb.2013.12.025 [arXiv:1307.3453 [hep-ph]].

[27] L. Yan and J. Y. Ollitrault, Phys. Rev. Lett. **112**, 082301 (2014) doi:10.1103/PhysRevLett.112.082301 [arXiv:1312.6555 [nucl-th]].

[28] M. G. Kendall, *The Advanced Theory of Statistics*, Charles Griffin and Company, London, 1945.

[29] F. G. Gardim, F. Grassi, M. Luzum and J. Y. Ollitrault, Phys. Rev. C **85**, 024908 (2012) doi:10.1103/PhysRevC.85.024908 [arXiv:1111.6538 [nucl-th]].

[30] D. Teaney and L. Yan, Phys. Rev. C **86**, 044908 (2012) doi:10.1103/PhysRevC.86.044908 [arXiv:1206.1905 [nucl-th]].

[31] F. G. Gardim, J. Noronha-Hostler, M. Luzum and F. Grassi, Phys. Rev. C **91**, no. 3, 034902 (2015) doi:10.1103/PhysRevC.91.034902 [arXiv:1411.2574 [nucl-th]].

[32] L. Yan and J. Y. Ollitrault, Phys. Lett. B **744**, 82 (2015) doi:10.1016/j.physletb.2015.03.040 [arXiv:1502.02502

[nucl-th]].

[33] J. Noronha-Hostler, L. Yan, F. G. Gardim and J. Y. Ollitrault, Phys. Rev. C **93**, no. 1, 014909 (2016) doi:10.1103/PhysRevC.93.014909 [arXiv:1511.03896 [nucl-th]].

[34] J. Noronha-Hostler, G. S. Denicol, J. Noronha, R. P. G. Andrade and F. Grassi, Phys. Rev. C **88**, no. 4, 044916 (2013) doi:10.1103/PhysRevC.88.044916 [arXiv:1305.1981 [nucl-th]].

[35] J. Noronha-Hostler, J. Noronha and F. Grassi, Phys. Rev. C **90**, no. 3, 034907 (2014) doi:10.1103/PhysRevC.90.034907 [arXiv:1406.3333 [nucl-th]].

[36] J. Noronha-Hostler, J. Noronha and M. Gyulassy, Phys. Rev. C **93**, no. 2, 024909 (2016) doi:10.1103/PhysRevC.93.024909 [arXiv:1508.02455 [nucl-th]].

[37] S. A. Bass *et al.*, Prog. Part. Nucl. Phys. **41**, 255 (1998) [Prog. Part. Nucl. Phys. **41**, 225 (1998)] doi:10.1016/S0146-6410(98)00058-1 [nucl-th/9803035].

[38] G. Aad *et al.* [ATLAS Collaboration], JHEP **1311**, 183 (2013) doi:10.1007/JHEP11(2013)183 [arXiv:1305.2942 [hep-ex]].

[39] N. Abbasi, D. Allahbakhshi, A. Davody, S. F. Taghavi, "To Appear"